EFFECT OF Co-Sm SUBSTITUTION ON NICKEL FERRITE SYNTHESIZED BY WOWS SOL-GEL METHOD

G. ASGHAR[a,*], M. RIAZ[a], S. N. KHUSRO[b], M. RASHID[a],
M. S. AWAN[c], G. H. TARIQ[d], F. SHABIR[a], M. A. UR REHMAN[e]
[a]*Department of Physics, The University of Poonch Rawalakot AJK*
[b]*Department of Physics,University of Kotli AJK*
[c]*Nano Sciences and Technical Division (NS & TD), National Centre for Physics (NCP), Islamabad*
[d]*Department of Physics, Khwaja Fareed University of Engineering & Information Technology, Rahim Yar Khan*
[e]*Applied Thermal Physics Laboratory, Department of Physics, COMSATS Institute of Information Technology, Islamabad 44000, Pakistan*

Cobalt and samarium substituted nickel spinel ferrite with general formula $Ni_{0.5}Co_{0.5-x}Sm_xFe_2O_4$ (x=0.0, 0.1, 0.2) is synthesized by the sol-gel (WOWS) technique. Phase formation and structural parameters are determined by using indexed XRD patterns. The results obtained from XRD patterns show the development of single phase spinel structure. The lattice parameter is found to decrease with doping concentration. The crystallite size of prepared nano particles is found to lie in the range 9nm to 23nm. The room temperature frequency dependent ac measurements are carried out in frequency range 20Hz to 3MHz. Dielectric loss is found to decrease with doping. Temperature varying dc electrical resistivity is measured in temperature range 110-400^{o}C and found to decrease with doping. Room temperature magnetic measurements show that coercivity decreases with doping.

(Received May 9, 2018; Accepted August 22, 2018)

Keywords: Spinel ferrites, Saturation magnetization, Electrical resistivity, Coercivity, Dielectric constant, Dielectric loss factor

1. Introduction

The unexpected non-trivial characteristics and potential applications of ferrite nanoparticles have attracted the attention of scientists since many decades. Among various applications, high storage magnetic devices, sensors, ferro fluids, magnetic resonance imaging, transformers, refrigeration systems and several other technological pillars are highly dependent on these materials [1-4]. Nanosized ferrites with spinel-type structure are among the most interesting materials since they exhibit properties different from those of the corresponding bulk phase materials [5].

Ni-ferrites are characterized by a spinel crystal structure that offers some flexibility on the occupancy of each site: on the cationic sites, atomic substitutions are allowed following a given set of rules, while the anionic sites can generally accommodate a few percent of vacancies [6]. Nickel ferrite ($NiFe_2O_4$) nanostructures has been widely studied and investigated for the potential application in the field of catalysis [7], magnetic data storage devices [8-11] and solid-oxide fuel cells [12-15]. Nickel ferrite nanostructures are synthesized through different physical and chemical methods employing nonchemical hard template [16], hydrothermal [17], ultrafast pyro-synthesis [18], chemical reduction [19], RF magnetron sputtering [20], auto-combustion [21] etc.

Typical spinel ferrites have general formula AB_2O_4. In this formula, A is divalent metal cation and B is trivalent Fe^{3+} ions. Eight AB_2O_4 formula units are present in one unit cell [22]. Apparently larger oxygen ions form a closed packed FCC structure with the smaller divalent metal

*Corresponding author: drghulamasghar@upr.edu.pk

cations occupying the interstitial positions. There are basically two types of interstitial sites in spinel ferrites; the tetrahedral A-site and the octahedral B-site occupied by the metal cations [23]. Scientists have tailored the properties of ferrites by using different dopants, occupying interstitial sites and by using different synthesis techniques.

Several techniques have been developed to prepare ferrite nanoparticles, including chemical co-precipitation, hydrothermal, citrate precursor technique, reverse micelle technique, plasma deposition method, pulsed wire discharge, high energy milling, mechanical alloying, microwave processing and sol gel method [24-30]. The sol-gel technique is widely used in synthesis of nanocrystalline ferrites due to small particle production, low synthesis temperature, and large rate of reaction [31].

In the present study, Co and Sm are doped in nickel ferrite having nominal composition $Ni_{0.5}Co_{0.5-x}Sm_xFe_2O_4$ (x=0.0, 0.1, 0.2). These ferrite nano particles have been synthesized by WOWS sol-gel technique. The main focus of this study is to investigate the effect of co-doping on structural, electrical and magnetic properties of $Ni_{0.5}Co_{0.5-x}Sm_xFe_2O_4$.

2. Synthesis

Samarium cobalt doped nickel spinel ferrite by general formula $Ni_{0.5}Co_{0.5-x}Sm_xFe_2O_4$ with x=0.0, 0.1, 0.2 was prepared by WOWS sol-gel technique. Firstly ethylene glycol is taken in 500ml of beaker for 5g sample preparation. $Ni(No_3)_2.6H_2O$ with the molecular weight 290.791g/mol is added in ethylene glycol and temperature is raised to 100^{o}C with constant stirring until it is completely dissolved. After dissolving it, $Co(No_3)_2.6H_2O$ with molecular weight 291.03g/mol is added to dissolve it in the solution at 100^{o}C and then $Fe(No_3)_3.9H_2O$ of molecular weight 404.00g/mol is added in the solution. The temperature of the solution is increased to 150^{o}C with continuous stirring to convert it into gel. The temperature of thick gel thus obtained is raised to 350^{o}C to burn the gel. The powder thus obtained after complete burning is ground well and some powder is converted to pellet by using hydraulic press. The powder and pellet are heat treated at 600^{o}C for 90 minutes and used for different characterizations.

3. Results and discussion

3.1 X-ray Diffraction (XRD)

All the diffraction peaks in XRD patterns are indexed with JCPDS card. Indexed XRD patterns of Sm-Co substituted nanocrystalline $NiFe_2O_4$ ferrites are shown in Fig. 1. The indexed patterns are indicative of spinel cubic crystal structure with the space group of Fd^3m.. The patterns show the presence of sharp, intense and well defined peaks and confirm the formation of highly crystalline single phase structure of doped spinel ferrite.

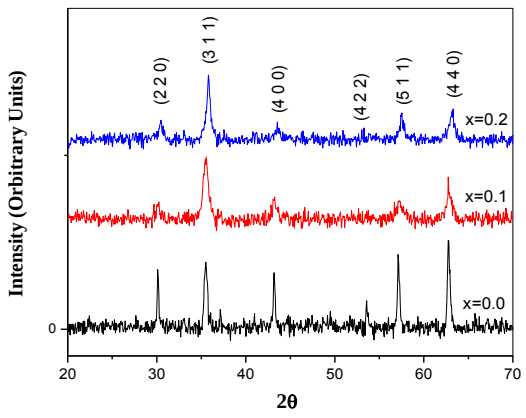

Fig. 1. Indexed XRD patterns of $Ni_{0.5}Co_{0.5-x}Sm_xFe_2O_4$ with x=0.0, 0.1, 0.2.

Structural parameters such as lattice constant (a), cell volume (V), crystallite size (D), X-ray density (Dx) calculated from the recorded XRD data are given in Table 1.

Table 1. Effect of Co-Sm on lattice parameter, unit cell volume, X-ray density, crystallite size.

Composition		x=0.0	x=0.1	x=0.2
1	Lattice Parameter(Å)	8.3665	8.3551	8.3149
2	Unit Cell volume ($Å^3$)	585.65	583.25	574.86
3	X-ray density (gcm^{-3})	5.319	5.551	5.84
4	Crystallite size (nm)	8.711	17.440	23.24
5	Bulk density (g/cm^3)	4.98	5.32	5.74

The lattice constants a and c are calculated using the following equation

$$\frac{1}{d^2} = \frac{4}{3}\left(\frac{h^2+hk+k^2}{a^2}\right) + \frac{l^2}{c^2} \quad (1)$$

where d is the inter planner spacing and (h k l) are the Miller indices of planes.

It can be seen from the table 1 that the lattice constant decreases with the increase in doping concentration of Sm-Cr. The decrease in value of lattice constant may be due to the occupancy of tetrahedral sites by Co^{2+} ions and the occupancy of rare-earth ion Sm^{3+} in B-sites instead of A site [32]. The increase in the Sm contents leads to continuous shift in 2θ towards a higher angle, which is corresponding to the decrease of lattice parameter.

Crystallite size can be measured by formula:

$$D=\frac{0.89\lambda}{\beta COS\theta} \quad (2)$$

where 'λ' is wavelength, β is FWHM and 'θ' is Bragg angle.

It is found that the average crystallite size of the ferrite nanoparticles is in the range 9-23 nm. The crystal size is increased with increase in Sm and Co concentration.

X-ray density is calculated by formula:

$$\rho_x = \frac{nM_m}{VN_A} \quad (3)$$

where 'n' is formula unit, 'M_m' is mass 'V' represents volume of unit cell and N_A is Avogadro's number.

It is found that X-ray density (ρ_x) is increased with Sm concentration which is due to its dependence on molecular weight and volume.

The unit cell volume is calculated by:

$$V = a^3 \quad (4)$$

The unit cell volume is found to decrease with the increase of Co and Sm concentration.

3.2 Dielectric Properties and dielectric loss tangent (tanΘ)

Dielectric Constant (ε′)

The ac electrical properties such as dielectric constant (ε′) for all the samples are measured in the frequency range of 20 Hz to 3MHz by using the values of capacitance (C) obtained from LCR meter and is shown in Fig. 2. The dielectric constant of the prepared samples is calculated by using the following relation

$$\varepsilon' = \frac{cd}{A\epsilon_o} \tag{5}$$

where, $A = \pi r^2$ = Area of the sample

c= Capacitance evaluated by LCR meter
d = Thickness
ε_0 = Absolute permittivity= 8.854×10^{-12} $C^2N^{-1}m^{-2}$

The variations of dielectric constant as a function of frequency for samples are shown in Fig. 2.

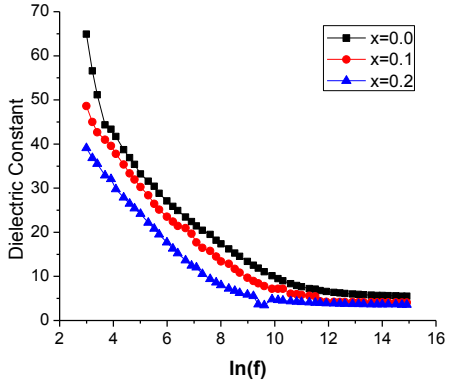

Fig. 2. Plot of dielectric constant with log of frequency of sintered samples.

It is clear that the dielectric constant decreases quickly by increasing frequency and becomes nearly constant at large frequencies. The decreased value of dielectric constant with increase in frequency is a usual dielectric behavior of spinel ferrites. The dielectric distribution curve can be explained on the basis of Koop's two-layer model and Maxwell-Wagner polarization theory.According to Koop, first layer is composed of inner region of large grains that acts as conducting layer at higher frequencies and the layer is of grain boundaries that act as highly resistive medium at lower frequencies. The polarization and conduction mechanism in ferrites are similar i.e. by electron exchange between ferrous (Fe^{2+}) and ferric (Fe^{3+}) ions [33].

The polarization takes place when electron hopes between ferrous (Fe^{2+}) and ferric (Fe^{3+}) ions. As the applied field frequency increases, it becomes harder for the electrons to hope from ferrous (Fe^{2+}) and ferric (Fe^{3+}) ions with the alternating frequency. This results in the decrease in net displacement of charge in one direction and hence dielectric constant decreases. It is observed that at relatively lower frequencies dielectric constant is high. It might be because of moisture, dislocations, voids, density and impurities [34]. Dielectric constant also decreases with the doping concentration. This is due to the fact that crystallite size increases with the increase in doping concentration given in Table 1. As the crystallite size increases, less charges accumulate on grain boundaries with the ac field and hence decreases the space charge polarization and results in the decrease in dielectric constant.

Table 2. Values of dielectric constant and dielectric loss.

Composition		x=0.0	x=0.1	x=0.2
1	Dielectric constant (100Hz)	36.894	33.3393	26.4810
2	Dielectric constant (3MHz)	5.4925	4.0645	3.5861
3	Dielectric loss at (100Hz)	1.3019	1.2785	0.9067
4	Dielectric loss at (3MHz)	0.0725	0.0421	0.0374

The Fig. 3 shows dielectric loss behavior of samples. It can be observed from Fig. 3 that dielectric loss has the similar trend as dielectric constant. The variation of dielectric loss with frequency showed same type of dispersion as in dielectric constant. At smaller frequencies, dielectric losses are higher and it decreases with increase in frequency and becomes almost constant up to 3MHz because of the high ac field decreases the value of polarization. As the frequency increases, the displacement of charges from one site to other site decreases. This reduces conduction and hence dielectric loss.

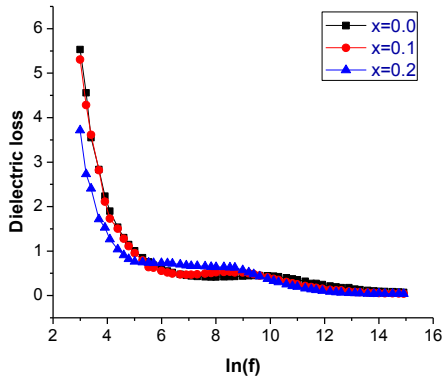

Fig. 3. Plot of dielectric losses with log of frequency of sintered samples.

3.3 D.C. electrical resistivity (ρ)

The temperature dependent dc resistivity measurements are determined by the two probe method. Variation in temperature dependent dc resistivity (ln ρ) with temperatures (1000/ T) for the prepared samples is illustrated in the Fig. 4. The plot shows that the dc resistivity decreases with increment of temperature indicated the semiconducting nature of the samples.

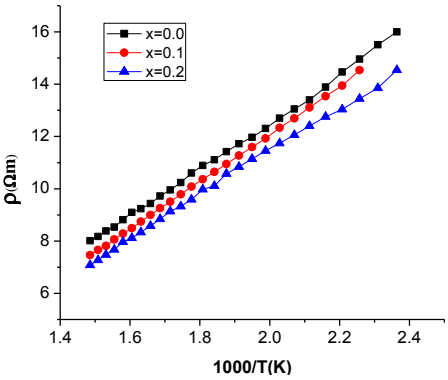

Fig. 4. Plot of ln ρ vs.100/T of prepared samples.

The decrease in dc resistivity with doping concentration is due to the increase in particle size. As particle size increases, grain boundaries decreases. The grain boundaries act as highly resistive medium. This resistive region decreases with increase in doping content and hence dc resistivity decreases.

3.4 Magnetic properties:

Magnetic properties of Sm-Co substituted nanocrystalline $NiFe_2O_4$ are studied by using vibrating sample magnetometer (VSM) at room temperature. The hysteresis loops of $Ni_{0.5}Co_{0.5-x}Sm_xFe_2O_4$, (x=0.0, 0.1, 0.2) are shown in Fig. 5(a), (b), (c). The magnetization curves represent the soft magnetic behavior of the ferrite samples. It is observed that saturation magnetization has decreased with increase in doping concentration. It may be due to replacement of Sm^{3+} ions (1μB) to Fe^{3+} (5μB) ions at B sites. Magnetisation in nickel ferrites is due to the difference in magnetic moment of ions present at B site and A site. As Sm^{3+} with less magnetic moment occupies B site so total magnetic moment at B site decreases and saturation magnetisation decreases. The hysteresis loops also show that with the increase in Sm^{3+} content, coercivity is decreasing. This decrease in coercivity is due to increase in grain boundaries with the increase in doping concentration.

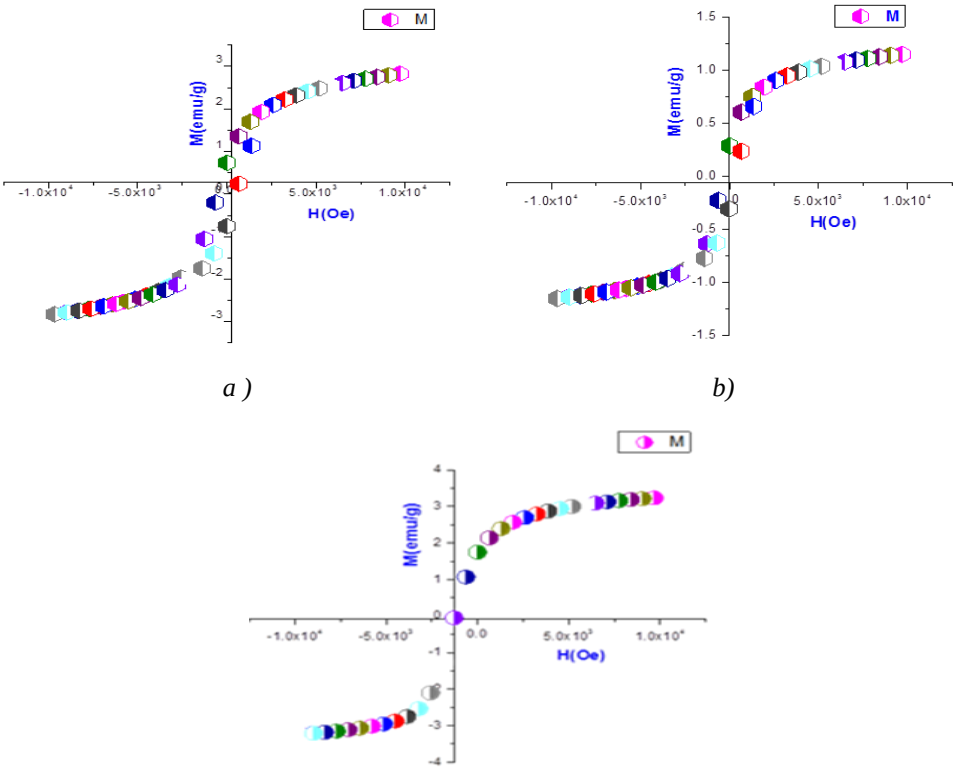

Fig. 5. Hysteresis loops of magnetization vs. applied field of prepared samples.

Table 3. Saturation magnetization (M_s), Remanance (M_r), Coercivity (H_c)

Composition	x=0.0	x=0.1	x=0.2
Ms (emu/gm.)	60.9491	48.8366	24.4439
Hc (Oe)	1243.3	500.30	357.94
Mr (emu/gm.)	32.7608	12.5225	6.04562

4. Conclusions

A series of cobalt and samarium substituted nickel spinel ferrites with general formula $Ni_{0.5}Co_{0.5-x}Sm_xFe_2O_4$ (x=0.0, 0.1, 0.2) has been successfully synthesized by the sol-gel method. Indexed XRD patterns are used for the structural characterization of the entire synthesized samples. The results of XRD investigation show the development of single phase spinel structure. The lattice parameter "a" is found to decrease with the increase in doping concentration.

The crystallite size of prepared nano particles is found to lie in the range 9nm to 23nm. The frequency dependent ac measurements are carried out at room temperature in frequency range 20Hz to 3MHz. Both dielectric constant and dielectric loss are found to decrease with the frequency as well as doping concentration. Temperature varying dc electrical resistivity is measured in temperature range 110-400^oC and found to decrease with doping indicating the semiconducting behavior. Room temperature magnetic measurements show that coercivity decreases with doping due to increase in crystallite size.

Acknowledgement

NanoScience and Technology Department, National Centre for Physics, Islamabad and Applied Thermal Physics Lab, COMSATS Institute of Information Technology Islamabad are acknowledged for their kind cooperation in this work.

References

[1] N. Ikenaga, Y. Ohgaito, H. Matsushima, T. Suzuki, Advances in the Science of Victorian Brown Coal Fuel fuel, **83** 661 (2004).
[2] N. Adeela, K. Maaz, U. Khan, M. Iqbal, S. Riaz, S. Naseem, Nanomaterials **6**, 73 (2016).
[3] J. P. Liu, Nanoscale Magnetic Materials and Applications, Springer **7**, 1032 (2009).
[4] N. A. Brusentsov, V. Gogosov, T. Brusentsova, A. Sergeev, N. Jurchenko, Journal of Magnetism and Magnetic Materials **225** 117 (2001).
[5] Tsvetomila Lazarova, Milena Georgieva, Dimitar Tzankov, Dimitrinka Voykova, Lyubomir Aleksandrov, Zara Cherkezova-Zheleva, Daniela Kovacheva, Journal of Alloys and Compounds **700**, 272 (2017).
[6] K. E. Sickafus, J. M. Wills, N. W. Grimes, Structure of spinel, J. Am. Ceram. Soc. **82**, 3279 (1999).
[7] P. Li, Z. Li, F. Zhai, Q. Wan, X. Li, X. Qu, A.A. Volinsky, J. Phys. Chem. C **117**, 25917 (2013).
[8] L. Li, G. Li, R. L. Smith, H. Inomata, Chem. Mater. **12**, 3705 (2000).
[9] V. Sepelak, I. Bergmann, A. Feldhoff, P. Heitjans, F. Krumeich, D. Menzel Fred, J. Litterst Stewart, J. Campbell Klaus, D. Becker, J. Phys. Chem. C **111**, 5026 (2007).
[10] J. Zhang, J. Fu, G. Tan, F. Li, C. Luo, J. Zhao, E. Xie, D. Xue, H. Zhang, N. J. Mellors, Y. Peng, Nanoscale **4**, 2754 (2012).
[11] G. Fan, X. Xiang, J. Fan, F. Li, J. Mater. Chem. **20**, 7378 (2010).
[12] C. T. Cherian, J. Sundaramurthy, M. V. Reddy, P. Suresh Kumar, K. Mani, D. Pliszka, C. H. Sow, S. Ramakrishna, B. V. R. Chowdari, ACS Appl. Mater. Interfaces **5**, 9957 (2013).
[13] S. Liu, F. He, Z. Huang, A. Zheng, Y. Feng, Y. Shen, H. Li, H. Wu, P. Glarborg, Energy Fuels **30**, 4251 (2016).
[14] P. Ramesh Kumar, S. Mitra, RSC Adv. **3**, 25058 (2013).
[15] J. Wang, G. Yang, L. Wang, W. Yan, J. Mater. Chem. A **4**, 8620 (2016).
[16] Y. Li, K. Guo, J. Li, X. Dong, T. Yuan, X. Li, H. Yang, ACS Appl. Mater. Interfaces **6**, 20949 (2014).
[17] Z.Y. Yu, L.F. Chen, S.H. Yu, J. Mater. Chem. A **2**, 10889 (2014).
[18] P. Preetham, M. Subhalaxmi, V.N. Shantikumar, S. Dhamodaran, R. Alok Kumar, RSC Adv. **6**, 38064 (2016).

[19] D. Carta, D. Loche, G. Mountjoy, G. Navarra, A. Corrias, J. Phys. Chem. C. **112**, 15623 (2008).
[20] C. Solis, S. Somacescu, E. Palafox, M. Balaguer, J. M. Serra, J. Phys. Chem. C **118**, 24266 (2014).
[21] J. Zhang, P. Li, Q. Wan, F. Zhai, A.A. Volinsky, X. Qu, RSC Adv. **5**, 81212 (2015).
[22] H. El Moussaoui, T. Mahfoud, S. Habouti, K. El Maalam, M. Ben Ali, M. Hamedoun, O. Mounkachi, R. Masrour, E. K. Hlil, A. Benyoussef, J. Magn. Magn. Mater. **405**, 181 (2016).
[23] S. A. Oliver, V. G. Harris, H. H. Hamdeh, J. C. Ho, Appl. Phys. Lett. **76**, 2761 (2000).
[24] Z. K. Heiba, Mohamed Bakr Mohamed, A. M. Wahba, L. Arda, Journal of Superconductivity and Novel Magnetism. **28**(8), 2517 (2015).
[25] Manish Srivastava, S. Chaubey, Animesh K. Ojha, Materials Chem. and Phys. **118**, 0174 (2009).
[26] V. Šepelák, D. Baabe, D. Mienert, D. Schultze, F. Krumeich, F. J. Litterst, K. D. Becker, J. Magn. Magn. Mater. **257**, 377 (2003).
[27] Y. T. Pavlyukhin, Y. Y. Medikov, V. V. Boldyrev, J. Solid State Chem. **53**, 155 (1984).
[28] P. Y. Lee, K. Ishizaka, H. Suematsu, W. Jiang, K. Yatsui, J. Nanopart. Res. **8**, 29 (2006).
[29] A. Kale, S. Gubbala, R.D.K. Misra, J. Magn. Magn. Mater. **277**, 350 (2004).
[30] M. De Marco, X. W. Wang, R. L. Snyder, J. Simmins, S. Bayya, M. White, M.J. Naughton, J. Appl. Phys. **73**, 6287 (1993).
[31] Tehrani, F. S., Daadmehr, V., Rezakhani, A. T., Akbarnejad, R. H., Gholipour, S. Journal of Superconductivity and Novel Magnetism **25**, 2443 (2012).
[32] S. Goud, N. Venkatesh, H. N. Kumar, V. P. Somaiah, R. B. Reddy, Journal of Applied Chemistry **8**, 38 (2015).
[33] M. J. Iqbal, M. N. Ashiq, Chem. Eng. J. **136**, 383 (2008).
[34] L. B. Kong, Z. W. Li, G. Q. Lin, Y. B. Gan, J. Am. Ceram. Soc. **90**(7)**,** 2104 (2007).